Zeitschrift: Helvetica Physica Acta
Band: 42 (1969)
Heft: 1

Artikel: Effect of nonlinear excitation on magnetoacoustic resonance in a cold plasma
Autor: Fässler, K. / Vaclavik, J. / Schneider, H.
DOI: https://doi.org/10.5169/seals-114053

Effect of Nonlinear Excitation on Magnetoacoustic Resonance in a Cold Plasma[1])

by **K. Fässler, J. Vaclavik**[2]) and **H. Schneider**
University of Fribourg, Department of Physics, Fribourg, Switzerland

(1. IV. 68)

Abstract. In magnetoacoustic resonance, amplification of the exciting magneting field was studied, both theoretically and experimentally, in the region where B_z is not small compared with magnetostatic field B_0. Dependence on the mutual polarity of B_0, B_z and on the exciting energy was found and excitation of higher harmonics was observed.

TABLE OF CONTENTS

I. Introduction

It has been theoretically found [1, 2] that in a cylindrical plasma surrounded by conducting walls amplitudes of linear magnetoacoustic waves can rapidly increase under certain conditions. In particular, when frequency of the exciting magnetic field approaches one of the natural frequencies of the plasma cylinder, the corresponding

[1]) Supported by the Swiss National Foundation for Scientific Research.
[2]) Permanent address: Czechoslovak Academy of Science, Institute of Plasma Physics, Prague.

mode is extremly excited and resonance occurs. This phenomenon is called magnetoacoustic resonance or space amplification of the exciting magnetic field.

Magnetoacoustic resonance has been experimentally discovered and investigated by a number of authors [3–5]. Maximal amplification of the exciting magnetic field was observed when the resonance condition was satisfied. In all these experiments, however, magnetoacoustic resonance was investigated only for 'electrodynamically' linear excitation, i.e. for amplitudes of the exciting magnetic field much smaller than those of the magnetostatic field.

In this paper we study properties of magnetoacoustic resonance, both theoretically and experimentally, in the region where the exciting field amplitude is not small compared with the magnetostatic field. First, a nonlinear theory of this phenomenon is developed, assuming that only the purely radial oscillations of the plasma cylinder are excited and taking into account the nonlinear terms up to the order $0(B^2)$ (B is the magnetic field found in linear approximation). An experiment on the magnetoacoustic waves propagating radially in the plasma cylinder is then described and detailed measurements of physical parameters in question are presented. Finally, the theoretical and the experimental results are compared and discussed.

II. Theory

1. *Formulation of the Problem and the Basic Equations*

We investigate the forced oscillations of a partially ionised plasma cylinder surrounded by conducting walls in a homogeneous static longitudinal magnetic field. The main problem consists in accounting for the nonlinear interaction between the oscillations.

The plasma is assumed to consist of two components ('plasma' and neutral gas) and its density as constant over the entire area of the cylinder. The examination is carried out in the cold plasma approximation, considering, however, dissipative processes, i.e., the finite conductivity of the plasma (collisions between electrons and ions) and collisions between ions and neutral particles. Moreover, we confine ourselves to the study of oscillations with low frequencies $\omega \ll k\,c,\ \omega_{ei},\ \omega_h$ (k is wave number; c, the velocity of light; ω_{ei}, collision frequency between electrons and ions; ω_h, hybrid frequency), i.e., we consider only magnetohydrodynamic oscillations.

Under the above-stated assumptions we may describe the plasma by means of the equations of two-component magnetohydrodynamics as follows [6].

$$\frac{\partial \varrho_l}{\partial t} + \operatorname{div}(\boldsymbol{v}_l \varrho_l) = 0 \qquad (l = p, n)\,, \tag{1}$$

$$\varrho_p \frac{\partial \boldsymbol{v}_p}{\partial t} + \varrho_p (\boldsymbol{v}_p \cdot \operatorname{grad})\, \boldsymbol{v}_p = (\boldsymbol{j} \times \boldsymbol{B})/c - \varrho_p\, \omega_{in}\, (\boldsymbol{v}_p - \boldsymbol{v}_n)\,, \tag{2}$$

$$\varrho_n \frac{\partial \boldsymbol{v}_n}{\partial t} + \varrho_n (\boldsymbol{v}_n \cdot \operatorname{grad})\, \boldsymbol{v}_n = \varrho_p\, \omega_{in}\, (\boldsymbol{v}_p - \boldsymbol{v}_n)\,, \tag{3}$$

$$\operatorname{rot} \boldsymbol{B} = 4\pi \boldsymbol{j}/c\,, \tag{4}$$

$$\operatorname{rot} \boldsymbol{E} + \frac{\partial \boldsymbol{B}}{\partial t}\, 1/c = 0\,, \tag{5}$$

$$\boldsymbol{j} = \sigma\, (\boldsymbol{E} + (\boldsymbol{v}_p \times \boldsymbol{B})/c)\,. \tag{6}$$

ϱ_p, ϱ_n are the mass densities of the plasma and the neutral gas respectively; $\boldsymbol{v}_p$, $\boldsymbol{v}_n$, the corresponding magnetohydrodynamic velocities; $\boldsymbol{E}$, $\boldsymbol{B}$, electric and magnetic fields; $\boldsymbol{j}$, the electric current density; ω_{in}, collision frequency between ions and neutral particles and $\overleftrightarrow{\sigma}$, tensor of conductivity.

On eliminating the quantities $\boldsymbol{j}$ and $\boldsymbol{E}$ by virtue of Equations (4) and (6) we can reduce the given system of equations to

$$\frac{\partial \varrho_l}{\partial t} + \operatorname{div}(\boldsymbol{v}_l \varrho_l) = 0, \tag{7}$$

$$\varrho_p \frac{\partial \boldsymbol{v}_p}{\partial t} + \varrho_p (\boldsymbol{v}_p \cdot \operatorname{grad}) \boldsymbol{v}_p = (\operatorname{rot} \boldsymbol{B} \times \boldsymbol{B})/(4\pi) - \varrho_p \omega_{in} (\boldsymbol{v}_p - \boldsymbol{v}_n), \tag{8}$$

$$\varrho_n \frac{\partial \boldsymbol{v}_n}{\partial t} + \varrho_n (\boldsymbol{v}_n \cdot \operatorname{grad}) \boldsymbol{v}_n = \varrho_p \omega_{in} (\boldsymbol{v}_p - \boldsymbol{v}_n), \tag{9}$$

$$\frac{\partial \boldsymbol{B}}{\partial t} + \operatorname{rot}(\overleftrightarrow{\eta} \operatorname{rot} \boldsymbol{B})\, c^2/(4\pi) - \operatorname{rot}(\boldsymbol{v}_p \times \boldsymbol{B}) = 0, \qquad \overleftrightarrow{\eta} \equiv \overleftrightarrow{\sigma}^{-1}. \tag{10}$$

For further considerations it is convenient to introduce a cylindrical system of coordinates r, ϕ, z. In order to simplify the whole problem we assume that the length of the plasma cylinder is infinite. Hence we can consider only the purely radial oscillations of the plasma, writing $\partial/\partial\phi \equiv \partial/\partial z \equiv 0$ in Equations (7) to (10). Furthermore we write

$$\boldsymbol{B} = \boldsymbol{B} + \tilde{\boldsymbol{B}}_0,\ \varrho_l = \varrho_{l0} + \tilde{\varrho}_l,\ \boldsymbol{v}_l \equiv \tilde{\boldsymbol{v}}_l,\ \boldsymbol{B}_0 \equiv (0, 0, B_0),$$

where the quantities with the subscript 0 are static and those with symbol $\sim$ are oscillating. Moreover, we have to specify the kind of excitation of the plasma oscillations. Consistently with the experimental arrangement, we assume that on the boundary of the plasma cylinder $r = R$ (R is radius of cylinder) a magnetic field of the following form is excited

$$\boldsymbol{B}(0, 0, \tilde{B}_{ex}(t)), \qquad \tilde{B}_{ex}(t) = B_{ex} \cos(\omega_0 t), \qquad B_{ex} = \text{const.} \tag{11}$$

Taking all these assumptions into account we considerably simplify Equations (7) to (10). Thus they are written as

$$\frac{\partial \tilde{\varrho}_l}{\partial t} + \frac{1}{r}\frac{\partial}{\partial r}(r \varrho_{l0} \tilde{v}_l) = -\frac{1}{r}\frac{\partial}{\partial r}(r \tilde{\varrho}_l \tilde{v}_l), \tag{12}$$

$$\frac{\partial \tilde{B}}{\partial t} - \frac{1}{r}\frac{\partial}{\partial r}\left(r \frac{\partial \tilde{B}}{\partial r}\right) \eta\, c^2/(4\pi) + \frac{B_0}{r}\frac{\partial}{\partial r}(r \tilde{v}_p) = -\frac{1}{r}\frac{\partial}{\partial r}(r \tilde{v}_p \tilde{B}), \tag{13}$$

$$\varrho_{p0} \frac{\partial \tilde{v}_p}{\partial t} + \frac{B_0}{4\pi}\frac{\partial \tilde{B}}{\partial r} + \varrho_{p0} \omega_{in} (\tilde{v}_p - \tilde{v}_n) = -\tilde{\varrho}_p \frac{\partial \tilde{v}_p}{\partial t} - (\varrho_{p0} + \tilde{\varrho}_p) \tilde{v}_p \frac{\partial \tilde{v}_p}{\partial r} - \tilde{B} \frac{\partial \tilde{B}}{\partial r}\Big/(4\pi) - \tilde{\varrho}_p \omega_{in} (\tilde{v}_p - \tilde{v}_n), \tag{14}$$

$$\varrho_{n0} \frac{\partial \tilde{v}_n}{\partial t} - \varrho_{p0} \omega_{in} (\tilde{v}_p - \tilde{v}_n) = -\tilde{\varrho}_n \frac{\partial \tilde{v}_n}{\partial t} - (\varrho_{n0} + \tilde{\varrho}_n) \tilde{v}_n \frac{\partial \tilde{v}_n}{\partial r} + \tilde{\varrho}_p \omega_{in} (\tilde{v}_p - \tilde{v}_n). \tag{15}$$

Here we have used the formulas $\eta_{\phi z} \equiv \eta_{z\phi} \equiv 0$ [6]; $\tilde{B} \equiv \tilde{B}_z$, $\tilde{v}_l \equiv \tilde{v}_{lr}$, $\eta \equiv \eta_{\phi\phi}$.

Finally, we transform the above equations into the Fourier representation. On inserting the expression

$$\tilde{B}(t) = \int_{-\infty}^{+\infty} B_\omega \exp(-i\,\omega\,t)\,d\omega\,,$$

for $\tilde{\varrho}_l$ and $\tilde{v}_l$ analogously, in Equations (12) to (15) and in the boundary condition (11) we obtain after some simple rearrangements:

$$-i\,\omega\,\varrho_{l\omega} + \frac{1}{r}\frac{d}{dr}(r\,\varrho_{l0}\,v_{l\omega}) = -\int d\omega'\,\frac{1}{r}\frac{d}{dr}(r\,\varrho_{l\omega'}\,v_{l\omega-\omega'})\,, \tag{16}$$

$$-i\,\omega\,B_\omega - \frac{1}{r}\frac{d}{dr}\left(r\,\frac{dB_\omega}{dr}\right)\eta\,c^2/(4\pi) + \frac{B_0}{r}\frac{d}{dr}(r\,v_{p\omega}) = -\int d\omega'\,\frac{1}{r}\frac{d}{dr}(r\,B_{\omega'}\,v_{p\omega-\omega'})\,, \tag{17}$$

$$\begin{aligned} &-i\,\omega\,\varrho_{p0}\,v_{p\omega} + \frac{B_0}{4\pi}\frac{dB_\omega}{dr} + \varrho_{p0}\,\omega_{in}\,(v_{p\omega} - v_{n\omega}) \\ &= -\int d\omega'\left\{-i\,\omega'\,v_{p\omega'}\,\varrho_{p\omega-\omega'} + \varrho_{p0}\,v_{p\omega'}\frac{dv_{p\omega-\omega'}}{dr} + \frac{B_{\omega'}}{4\pi}\frac{dB_{\omega-\omega'}}{dr}\right. \\ &\left. + \omega_{in}\,\varrho_{p\omega-\omega'}\,(v_{p\omega'} - v_{n\omega'})\right\} - \iint d\omega'\,d\omega''\,\varrho_{p\omega-\omega'-\omega''}\,v_{p\omega'}\frac{dv_{p\omega''}}{dr}\,, \end{aligned} \tag{18}$$

$$\begin{aligned} &-i\,\omega\,\varrho_{n0}\,v_{n\omega} - \varrho_{p0}\,\omega_{in}\,(v_{p\omega} - v_{n\omega}) = \int d\omega'\left\{i\,\omega'\,v_{n\omega'}\,\varrho_{n\omega-\omega'}\right. \\ &\left. - \varrho_{n0}\,v_{n\omega'}\frac{dv_{n\omega-\omega'}}{dr} + \omega_{in}\,\varrho_{p\omega-\omega'}(v_{p\omega'} - v_{n\omega'})\right\} \\ &- \iint d\omega'\,d\omega''\,\varrho_{n\omega-\omega'-\omega''}\,v_{n\omega'}\frac{dv_{n\omega''}}{dr}\,, \end{aligned} \tag{19}$$

$$B_{ex\omega} = \frac{B_{ex}}{2}\{\delta(\omega - \omega_0) + \delta(\omega + \omega_0)\}\,. \tag{20}$$

These equations together with the boundary condition (20) represent the basic set of equations for the given problem.

2. *Solution of the Equations in Linear Approximation*

To solve the set of equations derived in the foregoing section, we use, as is usually done in nonlinear problems, a perturbation method. We seek the solution of these equations in power series with the parameter $B_{ex}/B_0 < 1$, i.e., we write

$$B_\omega = B_\omega^{(1)} + B_\omega^{(2)} + \cdots, \tag{21}$$

analogously for $\varrho_{l\omega}$ and $v_{l\omega}$, and

$$B_{ex\omega} = \frac{B_{ex}}{2}\{\delta(\omega - \omega_0) + \delta(\omega + \omega_0)\} + 0 + \cdots. \tag{22}$$

We insert the expressions (21) in Equations (16) to (19). In first (linear) approximation these equations are reduced to

$$-i\,\omega\,\varrho_{l\omega}^{(1)}+\frac{1}{r}\,\frac{d}{dr}\,(r\,\varrho_{l0}\,v_{l\omega}^{(1)})=0\,, \tag{23}$$

$$-i\,\omega\,B_{\omega}^{(1)}-\frac{\eta\,c^2}{4\,\pi\,r}\,\frac{d}{dr}\left(r\,\frac{dB_{\omega}^{(1)}}{dr}\right)+\frac{B_0}{r}\,\frac{d}{dr}\,(r\,v_{p\omega}^{(1)})=0\,, \tag{24}$$

$$-i\,\omega\,\varrho_{p0}\,v_{p\omega}^{(1)}+\frac{B_0}{4\,\pi}\,\frac{dB_{\omega}^{(1)}}{dr}+\varrho_{p0}\,\omega_{in}\,(v_{p\omega}^{(1)}-v_{n\omega}^{(1)})=0\,, \tag{25}$$

$$-i\,\omega\,\varrho_{n0}\,v_{n\omega}^{(1)}-\varrho_{p0}\,\omega_{in}\,(v_{p\omega}^{(1)}-v_{n\omega}^{(1)})=0\,. \tag{26}$$

On eliminating the quantities $v_{l\omega}^{(1)}$ from Equation (24) by means of Equations (25) and (26), we obtain the only differential equation for the magnetic field $B_{\omega}^{(1)}$ [5]

$$\frac{1}{r}\,\frac{d}{dr}\left(r\,\frac{dB_{\omega}^{(1)}}{dr}\right)+K_{\omega}^2\,B_{\omega}^{(1)}=0\,, \tag{27}$$

the wave number K_{ω} being given by formulas

$$K_{\omega}^2=\left(\frac{\omega}{c_a}\right)^2\frac{g_{\omega}}{1-i\,\omega\,g_{\omega}\,c^2/(4\,\pi\,c_a^2\,\sigma)}\,,\qquad g_{\omega}=\frac{I\,(1+i\,x_{\omega})}{1+i\,I\,x_{\omega}}\,,$$
$$x_{\omega}=\frac{\omega_{in}}{(1-I)\,\omega}\,,\qquad \sigma=\eta^{-1}=I\,\frac{e^2\,N_0}{m\,\omega_{ei}}\,. \tag{28}$$

c_a is Alfvén velocity, $c_a^2=B_0^2/(4\,\pi\,\varrho_0)$; $\varrho_0=\varrho_{p0}+\varrho_{n0}$; I is the degree of ionisation $I=\varrho_{p0}/\varrho_0$; e, electron charge; m, electron mass and N_0, particle density. We assume that $\omega_{ce}\gg\omega_{ei}$ (ω_{ce} is the cyclotron frequency of the electron).

Considering the boundary condition (22) the solution of the Equation (27) is easily found as

$$B_{\omega}^{(1)}=\frac{B_{ex}}{2}\,\{\delta\,(\omega-\omega_0)+\delta\,(\omega+\omega_0)\}\,\frac{J_0(K_{\omega}\,r)}{J_0(K_{\omega}\,R)}\,. \tag{29}$$

J_0 is the Bessel function of the zeroth order.

For $v_{l\omega}^{(1)}$ and $\varrho_{l\omega}^{(1)}$ we obtain from the Equations (23), (25) and (26), in terms of $B_{\omega}^{(1)}$:

$$v_{p\omega}^{(1)}=-\frac{dB_{\omega}^{(1)}}{dr}\,i\,B_0/(4\,\pi\,\varrho_0\,\omega\,g_{\omega})\,,\qquad v_{n\omega}^{(1)}=\frac{dB_{\omega}^{(1)}}{dr}\,I\,B_0\,\varrho_0\,\omega_{in}\,D_{\omega}/(4\,\pi)\,,$$
$$\varrho_{p\omega}^{(1)}=B_{\omega}^{(1)}\,I\,B_0\,K_{\omega}^2/(4\,\pi\,\omega^2\,g_{\omega})\,,$$
$$\varrho_{n\omega}^{(1)}=B_{\omega}^{(1)}\,i\,I\,(1-I)\,\varrho_0^2\,\omega_{in}\,B_0\,D_{\omega}\,K_{\omega}^2/(4\,\pi\,\omega)\,, \tag{30}$$

D_{ω} is given by

$$D_{\omega}=\{\omega^2\,\varrho_0^2\,I\,(1-I)\,(1+i\,x_{\omega})\}^{-1}\,. \tag{31}$$

The time dependent solution for the magnetic field, in first approximation, is then given by the inverse Fourier transformation as

$$\tilde{B}_{\omega}^{(1)}(r,t)=B_{ex}\,Re\left\{\frac{J_0(K_{\omega_0}\,r)}{J_0(K_{\omega_0}\,R)}\,\exp(-i\,\omega_0\,t)\right\}. \tag{32}$$

3. *Solution of the Equations in Second Approximation*

Having found all the necessary quantities in linear approximation, we may now proceed to higher approximations. However, as will be seen in the forthcoming part,

the calculation of the magnetic field, even in the lowest nonlinear approximation, is very cumbersome. Therefore, we further confine ourselves to the second approximation. Nevertheless, we hope to obtain sufficiently general information on the influence of nonlinear phenomena upon the magnetic field.

The Equations (17) to (19) for second order quantities are

$$
\begin{aligned}
&- i\,\omega\, B_{\omega}^{(2)} - \frac{1}{r}\,\frac{d}{dr}\left(r\,\frac{dB_{\omega}^{(2)}}{dr}\right)\frac{\eta\, c^2}{4\pi} + \frac{B_0}{r}\,\frac{d}{dr}\,(r\, v_{p\omega}^{(2)}) \\
&= -\int d\omega'\,\frac{1}{r}\,\frac{d}{dr}\,(r\, B_{\omega'}^{(1)}\, v_{p\,\omega-\omega'}^{(1)})\,, \qquad (33)
\end{aligned}
$$

$$
\begin{aligned}
&- i\,\omega\,\varrho_{p0}\, v_{p\omega}^{(2)} + \frac{B_0}{4\pi}\,\frac{dB_{\omega}^{(2)}}{dr} + \varrho_{p0}\,\omega_{in}\,(v_{p\omega}^{(2)} - v_{n\omega}^{(2)}) \\
&= -\int d\omega'\left\{- i\,\omega'\, v_{p\omega'}^{(1)}\,\varrho_{p\,\omega-\omega'}^{(1)} + \varrho_{p0}\, v_{p\omega'}^{(1)}\,\frac{dv_{p\,\omega-\omega'}^{(1)}}{dr}\right. \\
&\left. + B_{\omega'}^{(1)}\,\frac{dB_{\omega-\omega'}^{(1)}}{dr}\,\frac{1}{4\pi} + \omega_{in}\,\varrho_{p\,\omega-\omega'}^{(1)}\,(v_{p\omega'}^{(1)} - v_{n\omega'}^{(1)})\right\}, \qquad (34)
\end{aligned}
$$

$$
\begin{aligned}
&- i\,\omega\,\varrho_{n0}\, v_{n\omega}^{(2)} - \varrho_{p0}\,\omega_{in}\,(v_{p\omega}^{(2)} - v_{n\omega}^{(2)}) \\
&= \int d\omega'\left\{i\,\omega'\, v_{n\omega'}^{(1)}\,\varrho_{n\,\omega-\omega'}^{(1)} - \varrho_{n0}\, v_{n\omega'}^{(1)}\,\frac{dv_{n\,\omega-\omega'}^{(1)}}{dr}\right. \\
&\left. + \omega_{in}\,\varrho_{p\,\omega-\omega'}^{(1)}\,(v_{p\omega'}^{(1)} - v_{n\omega'}^{(1)})\right\}. \qquad (35)
\end{aligned}
$$

The equations of mass conservation do not appear because the set of the Equations (33) to (35) does not include the quantities $\varrho_{l\omega}^{(2)}$.

We insert now the expressions of linear approximation (30) on the right sides of the Equations (33) to (35). Then eliminating the quantities $v_{l\omega}^{(2)}$ from Equation (33) by means of Equations (34) and (35) we obtain, after rather tedious rearrangements, again the only differential equation for the magnetic field

$$
\frac{1}{r}\,\frac{d}{dr}\left(r\,\frac{dB_{\omega}^{(2)}}{dr}\right) + K_{\omega}^2\, B_{\omega}^{(2)} = f_{\omega}(r)\,,
$$

$$
\begin{aligned}
f_{\omega}(r) \equiv\ & \frac{K_{\omega}^2\, B_0}{4\pi\,\omega\,\varrho_0}\int d\omega'\left\{B_{\omega'}^{(1)}\, B_{\omega-\omega'}^{(1)}\left(\frac{K_{\omega-\omega'}^2}{(\omega-\omega')\, g_{\omega-\omega'}} + \frac{K_{\omega'}^2}{\omega\, g_{\omega}}\right)\right. \\
&- \frac{dB_{\omega'}^{(1)}}{dr}\,\frac{dB_{\omega-\omega'}^{(1)}}{dr}\, K_{\omega-\omega'}^2\, I\, c_a^2\left(\frac{1}{(\omega-\omega')\, g_{\omega-\omega'}} + \frac{1}{\omega\, g_{\omega}}\right) \\
&+ K_{\omega-\omega'}^2\, I\, c_a^2\left(\frac{1}{\omega\,(\omega-\omega')^2\, g_{\omega}\, g_{\omega'}\, g_{\omega-\omega'}} + \frac{i\,\omega'\, D_{\omega'}\,\varrho_0^2\,\omega_{in}\,(1-I)}{\omega\,(\omega-\omega')^2\, g_{\omega}\, g_{\omega-\omega'}}\right. \\
&\left. + \omega'\,\omega_{in}^2\,\varrho_0^6\, D_{\omega}\, D_{\omega'}\, D_{\omega-\omega'}\, I\,(1-I)^2\right)\left(\frac{dB_{\omega'}^{(1)}}{dr}\,\frac{dB_{\omega-\omega'}^{(1)}}{dr}\right. \\
&\left. - K_{\omega'}^2\, B_{\omega'}^{(1)}\, B_{\omega-\omega'}^{(1)}\right) + \frac{1}{r}\,\frac{d}{dr}\left(r\,\frac{dB_{\omega'}^{(1)}}{dr}\,\frac{d^2B_{\omega-\omega'}^{(1)}}{dr^2}\right) \\
&\times I\, c_a^2\left(\frac{1}{\omega\,\omega'\,(\omega-\omega')\, g_{\omega}\, g_{\omega'}\, g_{\omega-\omega'}}\right. \\
&\left.\left. - i\,\omega_{in}^3\,\varrho_0^6\, I^2\,(1-I)\, D_{\omega}\, D_{\omega'}\, D_{\omega-\omega'}\right)\right\}. \qquad (36)
\end{aligned}
$$

Using (29) we are able to carry out the indicated integration. After some simple operations we arrive at the function $f_\omega(r)$ in the final form

$$
\begin{aligned}
f_\omega(r) = \frac{B_{ex}^2 c_a^2}{4 B_0} \Big\{ & \frac{K_{2\omega_0}^2}{2\omega_0 J_0^2(K_{\omega_0} R)} \Big(\alpha_{\omega_0} (J_0^2(K_{\omega_0} r) - J_1^2(K_{\omega_0} r)) \\
& + \beta_{\omega_0} \Big(\Big(\frac{J_1(K_{\omega_0} r)}{K_{\omega_0} r} \Big)^2 - \frac{J_0(K_{\omega_0} r)\, J_1(K_{\omega_0} r)}{K_{\omega_0} r} \Big) \Big) \delta(\omega - 2\omega_0) \\
& + \text{com. con. } \delta(\omega + 2\omega_0) + \frac{2}{c_a^2 |J_0(K_{\omega_0} R)|^2} (Re\, \varepsilon_{\omega_0} |J_0(K_{\omega_0} r)|^2 \\
& + Re\, \eta_{\omega_0} |J_1(K_{\omega_0} r)|^2 + \Lambda_{\omega_0} \Big(\Big| \frac{J_1(K_{\omega_0} r)}{K_{\omega_0} r} \Big|^2 \\
& - Re \Big(\frac{\bar{J}_0(K_{\omega_0} r)\, J_1(K_{\omega_0} r)}{K_{\omega_0} r} \Big) \Big) \Big) \delta(\omega) \Big\}. \qquad (37)
\end{aligned}
$$

J_1 is the Bessel function of the first order, the bar denotes complex conjugated quantities, and the coefficients α_ω, β_ω, etc. are given by

$$
\begin{aligned}
\alpha_\omega &= \frac{K_\omega^2}{\omega} \Big(\frac{1}{g_\omega} + \frac{1}{2 g_{2\omega}} \Big) - K_\omega^4 I c_a^2 \Big(\frac{i D_\omega \varrho_0^2 \omega_{in} (1-I)}{2\omega^2 g_\omega g_{2\omega}} \\
&\quad + D_\omega^2 D_{2\omega} \varrho_0^6 \omega_{in}^2 I (1-I)^2 \omega (1 + i x_\omega I) \Big), \\
\beta_\omega &= 2 I c_a^2 K_\omega^4 \Big(\frac{1}{2\omega^3 g_\omega^2 g_{2\omega}} - i \omega_{in}^3 \varrho_0^6 I^2 (1-I) D_\omega^2 D_{2\omega} \Big), \\
\varepsilon_\omega &= K_\omega^2 - |K_\omega|^4 I c_a^2 \Big(\frac{2}{\omega^2 |g_\omega|^2} + \frac{i D_\omega \varrho_0^2 \omega_{in} (1-I)}{\omega \bar{g}_\omega} \\
&\quad - i |D_\omega|^2 \varrho_0^4 \omega_{in} (1-I)^2 \omega (1 + i x_\omega I) \Big), \\
\eta_\omega &= |K_\omega|^2 \Big(\bar{K}_\omega^2 I c_a^2 \Big(\frac{2}{\omega^2 g_\omega^2} + \frac{i D_\omega \varrho_0^2 \omega_{in} (1-I)}{\omega \bar{g}_\omega} \\
&\quad - i |D_\omega|^2 \varrho_0^4 \omega_{in} (1-I)^2 \omega (1 + i x_\omega I) \Big) - 1 \Big), \\
\Lambda_\omega &= -2 I c_a^2 |K_\omega|^4 \Big(\frac{1}{\omega^2 |g_\omega|^2} + \omega_{in}^2 \varrho_0^4 I (1-I) |D_\omega|^2 \Big). \qquad (38)
\end{aligned}
$$

The Equation (36) is an inhomogeneous Bessel equation. The solution of such an equation can be found by virtue of a Green function [7]. Using the boundary condition (22), i.e. $B_\omega^{(2)} = 0$ on $r = R$, we find the following solution of Equation (36)

$$
B_\omega^{(2)}(r) = 2 \sum_{l=1}^{\infty} \frac{J_0(k_l r)}{J_1^2(\gamma_l)(K_\omega^2 - k_l^2)} \int_0^1 J_0(\gamma_l \xi)\, f_\omega(R\xi)\, \xi\, d\xi, \qquad (39)
$$

where $k_l = \gamma_l / R$ and γ_l are the zeros of the equation $J_0(x) = 0$.

Inserting the expression (37) in this formula and carrying out the inverse Fourier transformation, we finally get the complete time dependent solution for the magnetic field in second approximation as

$$
\begin{aligned}
\tilde{B}^{(2)}(r,t) = \frac{B_{ex}^2 c_a^2}{B_0} \sum_{l=1}^{\infty} \frac{J_0(k_l r)}{J_1^2(\gamma_l)} \Big\{ & \frac{1}{2\omega_0} Re \Big(\frac{K_{2\omega_0}^2 (\alpha_{\omega_0} I_1 + \beta_{\omega_0} I_2)}{J_0^2(K_{\omega_0} R)(K_{2\omega_0}^2 - k_l^2)} \\
& \times \exp(-i 2\omega_0 t) \Big) - \frac{1}{c_a^2 k_l^2 |J_0(K_{\omega_0} R)|^2} (Re\, \varepsilon_{\omega_0} I_3 + Re\, \eta_{\omega_0} I_4 + \Lambda_{\omega_0} I_5) \Big\}. \qquad (40)
\end{aligned}
$$

I_1, I_2, etc. denote integrals of combinations of the Bessel functions; they are given by

$$I_1 = \int_0^1 J_0(\gamma_l x)\,\{J_0^2(K_{\omega_0} R x) - J_1^2(K_{\omega_0} R x)\}\, x\, dx\,,$$

$$I_2 = \int_0^1 J_0(\gamma_l x)\left\{\left(\frac{J_1(K_{\omega_0} R x)}{K_{\omega_0} R x}\right)^2 - \frac{J_0(K_{\omega_0} R x)\, J_1(K_{\omega_0} R x)}{K_{\omega_0} R x}\right\} x\, dx\,,$$

$$I_3 = \int_0^1 J_0(\gamma_l x)\,|\,J_0(K_{\omega_0} R x)\,|^2\, x\, dx\,,$$

$$I_4 = \int_0^1 J_0(\gamma_l x)\,|\,J_1(K_{\omega_0} R x)\,|^2\, x\, dx\,,$$

$$I_5 = \int_1^0 J_0(\gamma_l x)\left\{\left|\frac{J_1(K_{\omega_0} R x)}{K_{\omega_0} R x}\right|^2 - Re\left(\frac{\bar{J}_0(K_{\omega_0} R x)\, J_1(K_{\omega_0} R x)}{K\omega_0 R x}\right)\right\} x\, dx\,. \tag{41}$$

4. *Discussion of the Results*

It is evident that the complete magnetic field $B(r, t)$ of the plasma oscillations in question is given, within the framework of the approximation considered, by the superposition of the magnetic fields (32) and (40). Since the integrals I_1, I_2, etc. (Equation (41)), which are included in the expression (40), are not to be found analytically, we have to use numerical methods to analyse the behaviour of the resultant magnetic field in dependence on various physical parameters. To simplify the problem we discuss here, as well as in the experimental part, only the magnetic field on the axis of the plasma cylinder. Thus we can write the expression for the 'normalised' magnetic field in a more convenient form

$$\begin{aligned} B_N(\tau) \equiv \frac{\tilde{B}(0, t)}{B_{ex}} &= \frac{\cos\tau}{|J_0(K_{\omega_0} R)|} + \frac{B_{ex}}{B_0}\,\frac{1}{|J_0(K_{\omega_0} R)|^2} \\ &\times \sum_{l=1}^{\infty} \frac{1}{J_1^2(\gamma_l)} \left\{ \frac{c_a^2}{2\,\omega_0\,|K_{2\omega_0}^2 - k_l^2|^2}\,(Re\, M_{\omega_0} \cos 2\,\tau + Im\, M_{\omega_0} \sin 2\,\tau) \right. \\ &\left. - \frac{1}{k_l^2}\,(Re\,\varepsilon_{\omega_0} I_3 + Re\,\eta_{\omega_0} I_4 + \Lambda_{\omega_0} I_5) \right\}, \end{aligned} \tag{42}$$

the quantity M_ω being given by

$$M_\omega = K_{2\omega}^2\,(\bar{K}_{2\omega}^2 - k_l^2)\,(\alpha_\omega I_1 + \beta_\omega I_2) \tag{43}$$

and

$$\tau = \arg J_0(K_{\omega_0} R) + \omega_0 t\,.$$

It can be immediately seen that the magnetic field (42) has, in dependence on various parameters, a resonance character caused not only by the denominator $|J_0(K_{\omega_0} R)|$, which is a well-known fact in the linear theory of magnetoacoustic resonance, but also by the denominator $|K_{2\omega_0}^2 - k_l^2|$, which describes resonances between the second harmonics of the plasma oscillations and the proper frequencies of the plasma cylinder. Consequently, the nonlinear interaction of the oscillations

considered brings about new resonances in the system. All further conclusions concerning the behaviour of the magnetic field can be arrived at only by using a computer.

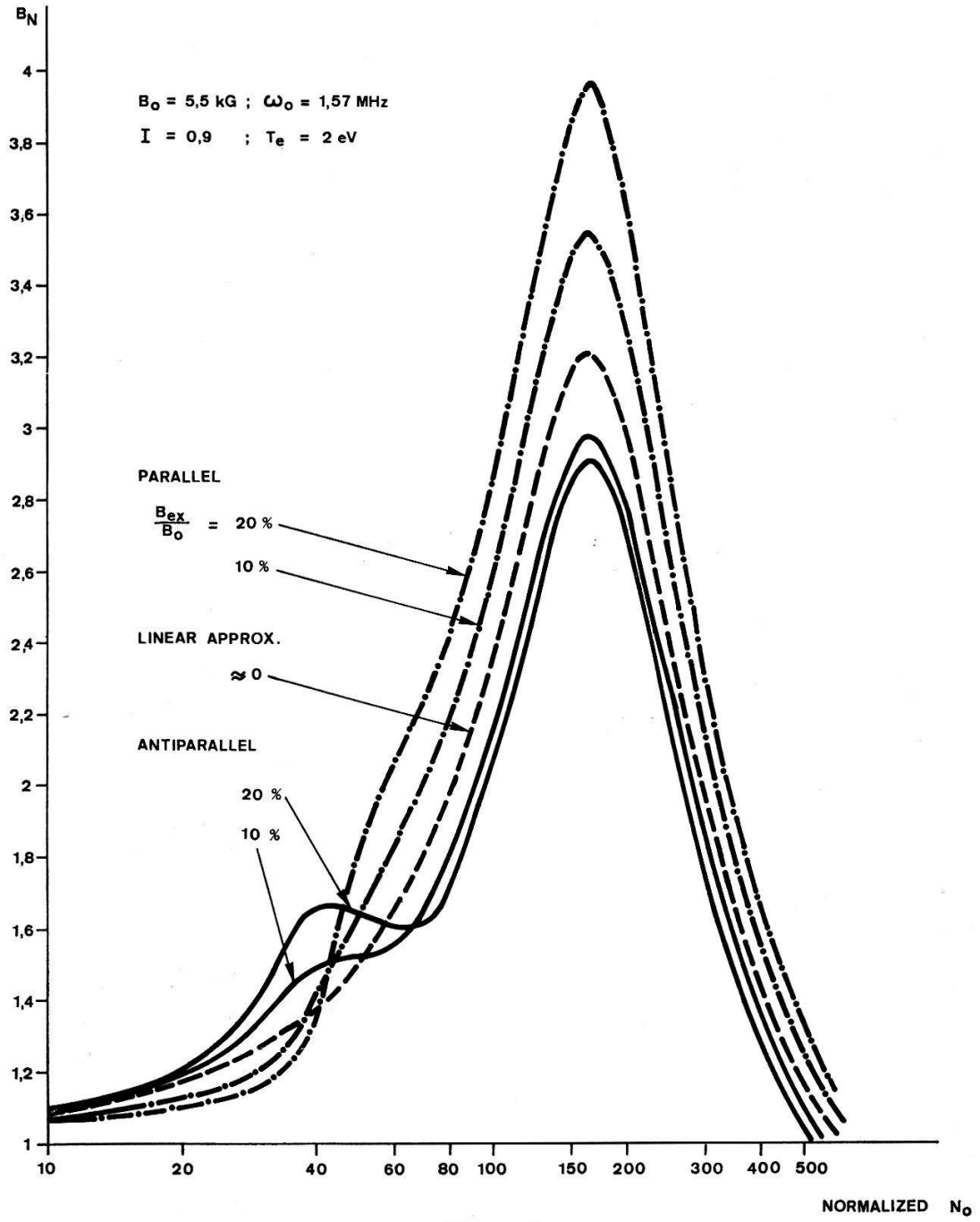

Figure 1

Resonance curves of B_N for argon plasma as a function of normalised plasma density N_0. The parameter of the curves is the ratio B_{ex}/B_0.

We computed the maximal amplitude (maximal with respect to the 'time' τ) of the magnetic field B_N in two cases: within the half period when the excited magnetic field on the boundary of the cylinder and the static magnetic field B_0 are parallel, and within the half period when they are antiparallel. The results are given in Figures 1, 2 and in Figures 7a, 8a, 9a and 10a of Chapter 4.

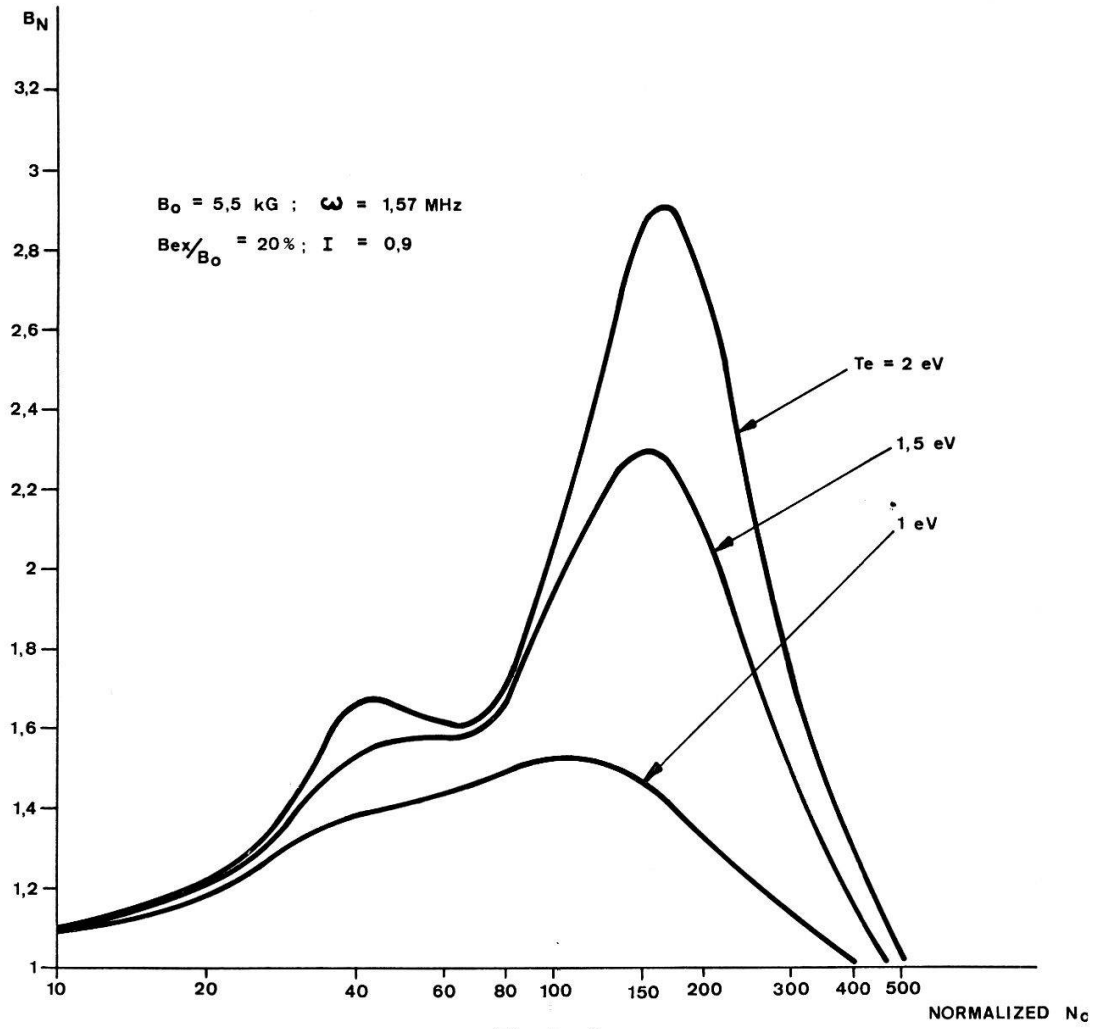

Figure 2

Resonance curves of B_N for argon plasma as a function of N_0. The parameter of the curves is the electron temperature T_e.

III. Experiment

In a cylindrical glass tube with an axial magnetostatic field B_0, a highly ionised argon plasma is generated by a gas discharge. In the afterglow, an oscillating current I_ϕ on the cylinder wall excites a magnetic field B_z. This field induces, inside the plasma, magnetoacoustic waves propagating radially.

1. *Discharge Apparatus*

The arrangement of the apparatus is shown schematically in Figure 3. It consists essentially of the discharge tube, the coil for the magnetic field and the excitation coil.

1.1. Discharge Tube

The discharge tube is a 78 cm long pyrex glass cylinder, with an inner diameter of 7,4 cm. The hollow electrodes are made of stainless steel and the end plates of pyrex. The tube is evacuated up to 10^{-5} mm Hg; then argon gas flows continously through the tube. The pressure of gas is variable between 30 and 1000 μHg. Below 180 μHg it is measured by a membrane micromanometer, above 180 μHg by a McLeod manometer using a cooling device between the discharge tube and the manometer.

The discharge current is generated by a 3,85 kJ condenser bank. The circuit is critically damped by an ohmic resistance ($R = 0{,}25\,\Omega$). The switching on of the bank across the electrodes causes ionisation and ohmic heating of the gas. The current reaches its maximum of 25 kA in 10 μsec and flows during 70 μsec.

1.2. Magnetostatic Field

The discharge tube is mounted in a coil which serves to generate the magnetostatic field. Fields of comparable strength are built up in this coil and in the single-turn excitation coil. Therefore, the inductive coupling of these coils has to be as small as possible; this can be realised by using a great flux ratio and a small winding ratio. The properties of the B_0-coil and the circuit are determined by this requirement, by the period desired and by the field.

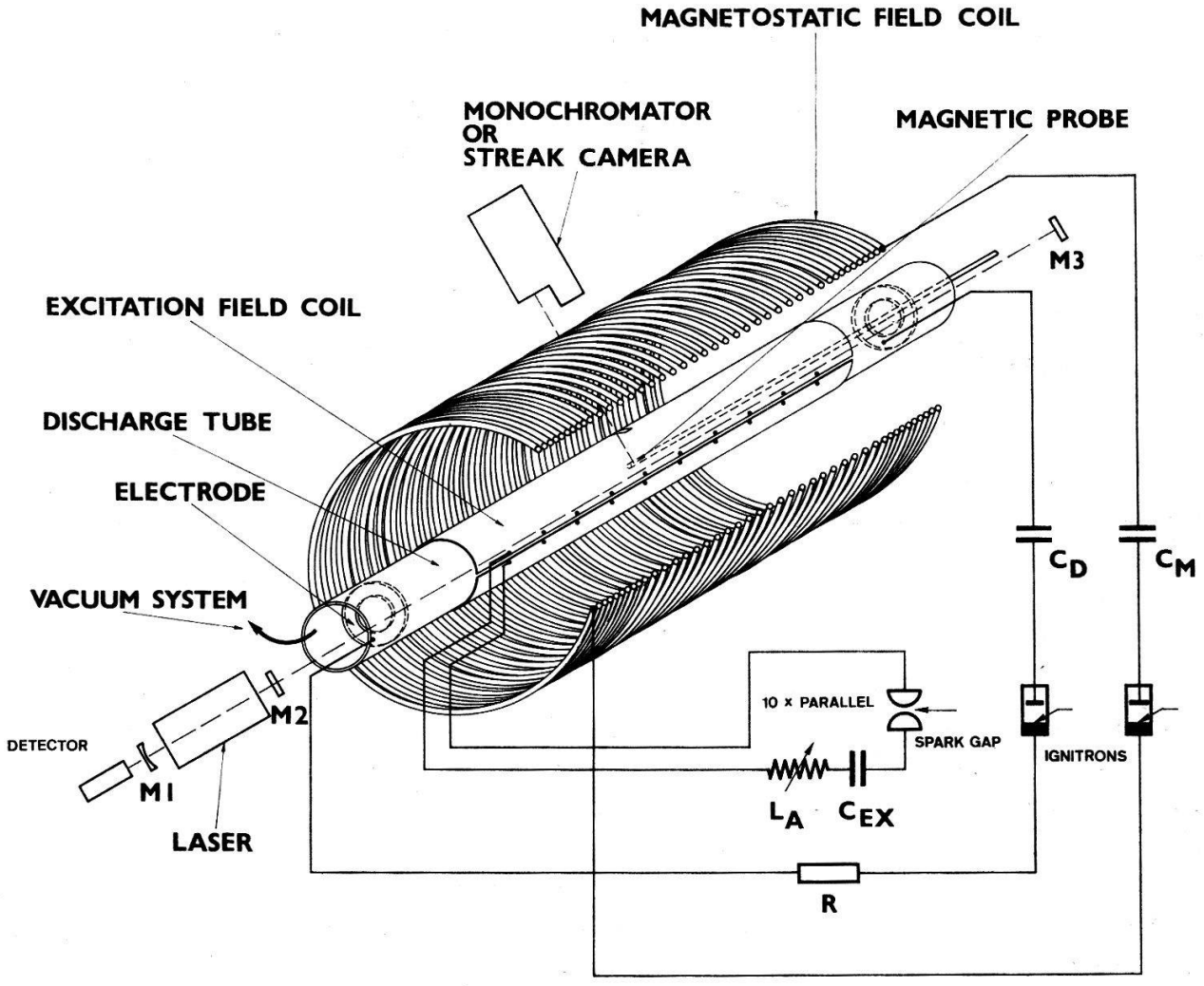

Figure 3

Schematic diagram of the experimental apparatus.

The coil has 42 windings, a length of 46 cm and a diameter of 33 cm. The windings are denser at each end than in the middle; this provides better field homogeneity. The condenser bank of $C_M = 740\,\mu$F is discharged through a collector and the coil. The polarity of the field can be altered by changing the coil connections. The magnetic field is varied between 3 and 6 kG and has a period of 2,1 msec. The deviation from

homogeneity was measured in radial direction over the glass tube area and found to be smaller than 0,2%, and in axial direction smaller than 0,5% 12 cm from midplane.

1.3. Excitation Circuit

The discharge tube is surrounded by a stainless steel single-turn coil, 0,5 mm thick and 50 cm long. For designing the oscillation circuit, its frequency, energy and voltage have to be given. In [8] was shown that the optimal arrangement is a parallel connection of several circuits discharged simultaneously through the excitation coil. Each circuit consists of a cable, a spark gap, a capacity $C_{ex} = 1\ \mu$F and an additional inductivity L_A which can be changed within the interval 0–0,5 μHenry and which permits variation of the excitation frequency. The cable connections are distributed equidistantly along the coil so that the current I_ϕ is distributed homogeneously. An axial field from 0,2 to 4 kG with frequencies from 0,8 to 1,57 MHz is generated by this current. Without plasma, the deviation from the homogeneity is in radial direction less than 0,2%, in axial direction less than 1% 17,5 cm from midplane.

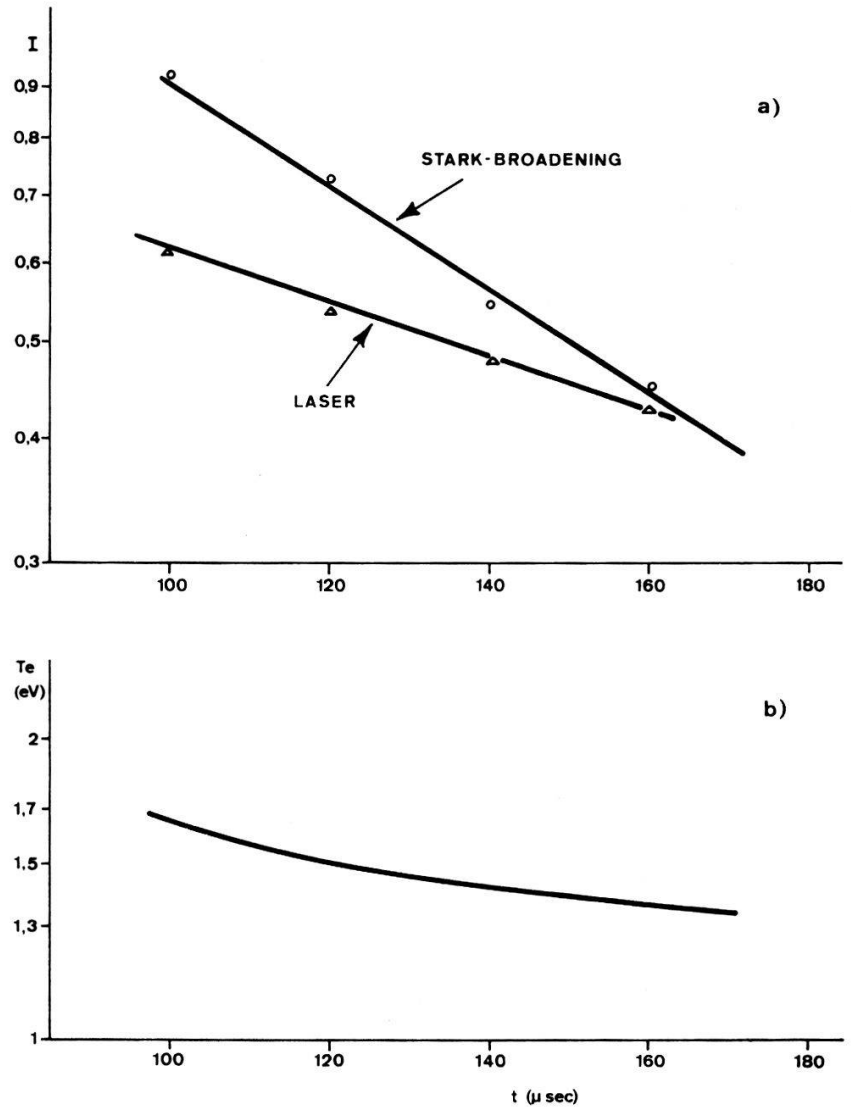

Figure 4

a) Time dependence of degree of ionisation. b) Time dependence of electron temperature. The horizontal scale refers to the start of the gas discharge.

1.4. Time Sequence of the Discharges

Figure 12 shows an oscillogramm of the time sequence of build up of the B_0-field, the gas discharge and the excitation for a typical example. The gas discharge is switched on 420 μsec after the start of the B_0-field. The frozen-in axial magnetostatic field prevents pinching of the gas column. Consequently, in the afterglow which starts after 490 μsec, the plasma contains fewer impurities, is well reproducible and decays slower. At 520 μsec, when the B_0-field reaches its maximal value, the magnetoacoustic waves are excited inside the plasma. At this stage of the afterglow the plasma parameters change so slowly that they can be regarded as constant within the first half-period of excitation. The B_0-field changes less than 0,2% during this time.

2. *Diagnostics*

In order to compare the theoretical and experimental results all plasma parameters have to be determined. For the same reason it is necessary to know how exactly the theoretical model of a uniform plasma filling the whole tube is realised. Furthermore, we have to verify whether the wave changes the parameters which are considered as constant in the theory. The arrangement of the diagnostic apparatuses is shown schematically in Figure 3.

2.1. Spectroscopic Measurement

Spectroscopic diagnostics are applied to determine the degree of ionisation and the temperature of the plasma. By measuring Stark-broadening of the H_β-line (mixing argon with 1,35% methane) in the afterglow, the electron density n_e can be determined from the half-width of the lines [5]. Provided that only single ionised atoms are present, n_e is equal to the ion density. Moreover, we measure the line intensity of different argon lines as a function of time and we determine the temperature of the gas

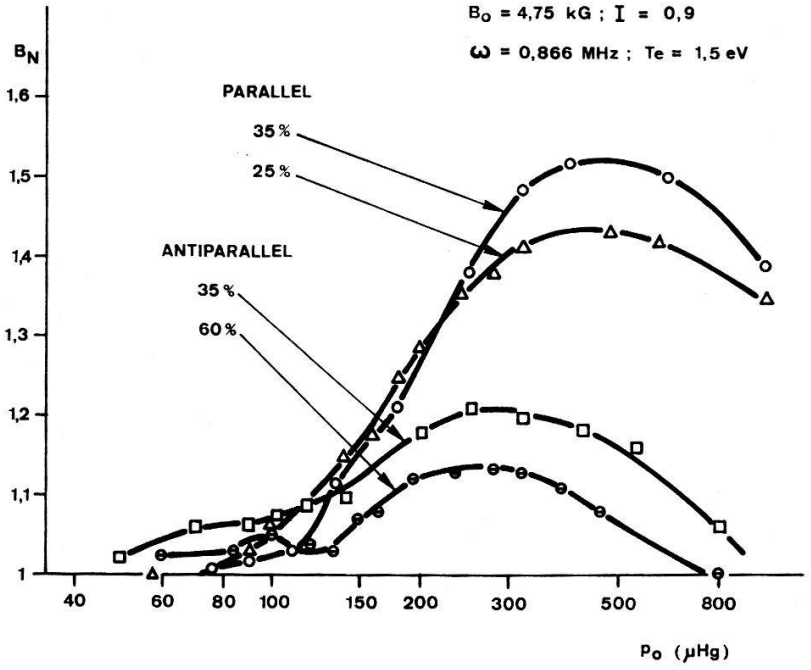

Figure 5

Experimental curves of B_N as a function of p_0. The parameter of the curves is $B_z(r = R)/B_0$ [%].

by norm temperature method. This method uses the fact that, for a given pressure, the line intensity as a function of time has a maximum which corresponds to a temperature defined as norm temperature [9].

Time spread spectroscopic measurements are made with an Ebert monochromatoı (Jarell-Ash, focus 0,5 m). A RCA 1P28 photomultiplier is used as a detector. It is screened against electromagnetic disturbances by a 5 mm ferromagnetic iron cylinder and a brass box which is connected to a Faraday cage by a copper shield.

2.2. Streak Camera

Time spread photographic pictures of the gas discharge and the excitation are made with a streak camera. Information is thus obtained on the light intensity change of the gas column and its dynamical behaviour. In the afterglow the influence of the wave on light intensity of the undisturbed plasma is photographed. Conclusions concerning the temperature change are made. For high energy excitation a shock wave is observed.

The camera has an object-glass with a focus of 600 mm, aperture 5,6. The maximal writing velocity is 5 mm/μsec. A polaroid camera or 6 $\times$ 60 cm^2 film-holder is mounted in the mirror plane so that plasma may be observed during 120 μsec.

2.3. Laser Interferometer

A He-Ne gas laser is used for measuring the electron density in axial direction. The laser works as an interferometer ($\lambda = 6328$ Å) according to the method of ASHBY and JEPHCOTT [10]. The modulated laser beam is registered by a photo diode, the signal of which is photographed on the oscillograph by a polaroid camera.

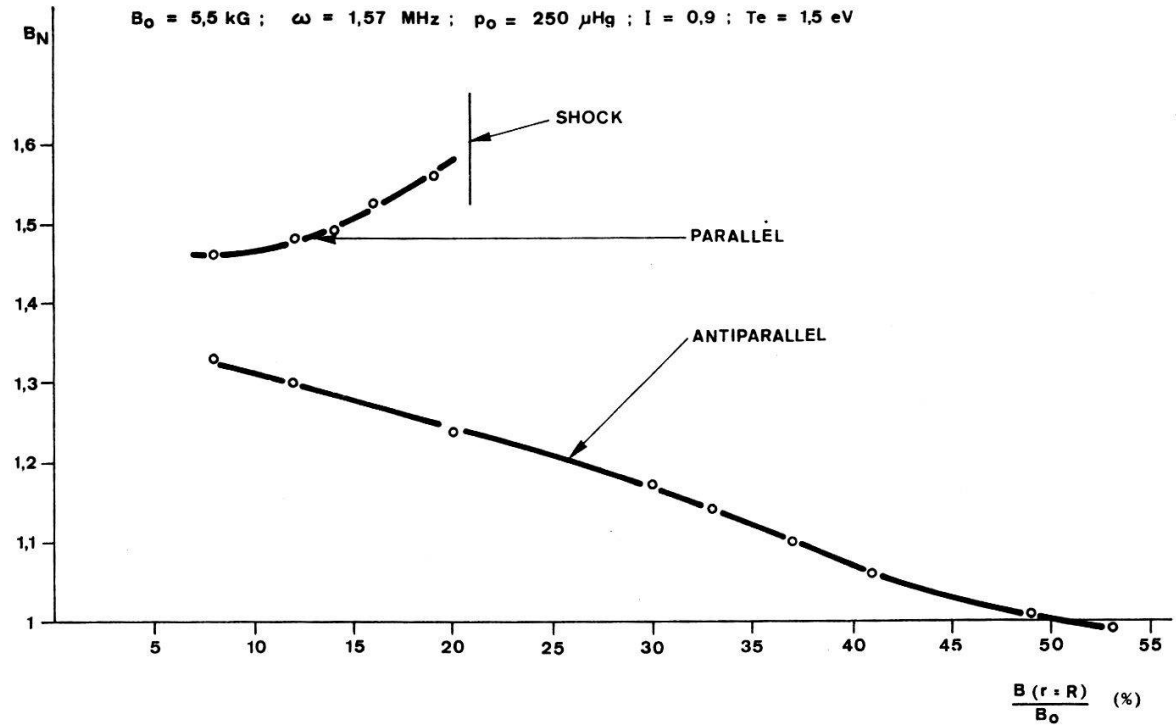

Figure 6

Experimental curves of B_N in the resonance as a function of $B_z(r = R)/B_0$.

2.4. Magnetic Probes

The magnetic fields are measured in a pyrex glass tube on the cylinder axis by electrostatically screened miniature probes (100 windings, diameter 2 mm). The probes are in the centre of the discharge tube. The signals induced in the probes are RC integrated and measured by the same method as in Sect. 2.3. The excitation field is comparable with the magnetostatic one. Therefore, the D.C. level of the magnetostatic field superposed on the excitation signal can be compensated on the oscillograph; high pass filters are not necessary.

IV. Results

1. *Degree of Ionisation and the Electron Temperature of the Undisturbed Plasma in the Afterglow*

The measurements of the Stark-broadening of the H_β-line permits determination of the time and the pressure dependence of the degree of ionisation. The pressure dependence shows that between 80 and 600 μHg the degree of ionisation decreases 5%. The theoretical as well as the experimental resonance curves are not sensitive to such a change. Thus the degree of ionisation can be regarded as constant. The time dependence of the degree of ionisation is shown in Figure 4a. The upper curve represents the results of the Stark-broadening measurement, the lower one the axial measurement made by the He-Ne gas laser. The values of the latter are at most 30% lower than those of the former. This discrepancy may be explained by the following argument: If the electron density decreases near the cylinder ends, the laser measurements will result in too low values, because the laser method gives an average value of the electron density along the path of the laser beam in the plasma.

Axial laser measurements across the radius of the discharge tube show that in the afterglow the plasma density can be regarded as constant over the entire area of the cylinder except for a small layer of 5 mm thickness near the wall.

The electron temperature was determined by means of the formula $I(1-I) = 0{,}9 \times 10^7 \exp(-E_i/T_e)/(E_i/T_e)^2$ using the measured values of the degree of ionisation. $E_i = 15{,}68$ eV is the ionisation energy of argon, T_e the electron temperature [5]. The time dependent behaviour of T_e is shown in Figure 4b. The values T_e were also measured by the norm temperature method. Within the time interval in question, i.e. 100–200 μsec, only A_{II}-lines provide a maximal intensity. For the 4348 line the norm temperature is 1,3 eV; the maximum was found after 135 μsec. This value is 10% lower than the corresponding value taken from the above-mentioned formula.

2. *Resonance Curves*

From the theoretical treatment it follows that the condition of magnetoacoustic resonance is roughly given by the formula $P_{0res} = A\, B_0^2/\omega$, where A is a constant determined by the radius of the plasma cylinder and by the kind of gas and p_{0res} is the resonance gas pressure. In the experiment B_0 and ω were chosen as parameters so that resonance might occur in a reasonable pressure region. Since the main problem of the work consists of studying nonlinear effects, resonance curves were measured for exciting magnetic fields B_z of different magnitudes which were not small compared with the magnetostatic field. The amplitudes of the oscillating magnetic fields in

plasma were measured on the axis of the cylinder in two different cases: B_0, B_z having once the same and then inverse polarity within the first half-period of excitation. The measured values of the magnetic fields are given as normalised values $B_N = B_z\,(r = 0)/B_z\,(r = R)$, where $B_z\,(r = 0)$ and $B_z\,(r = R)$ are the maximal values of the oscillating fields within the first half-period on the axis and on the wall, respectively.

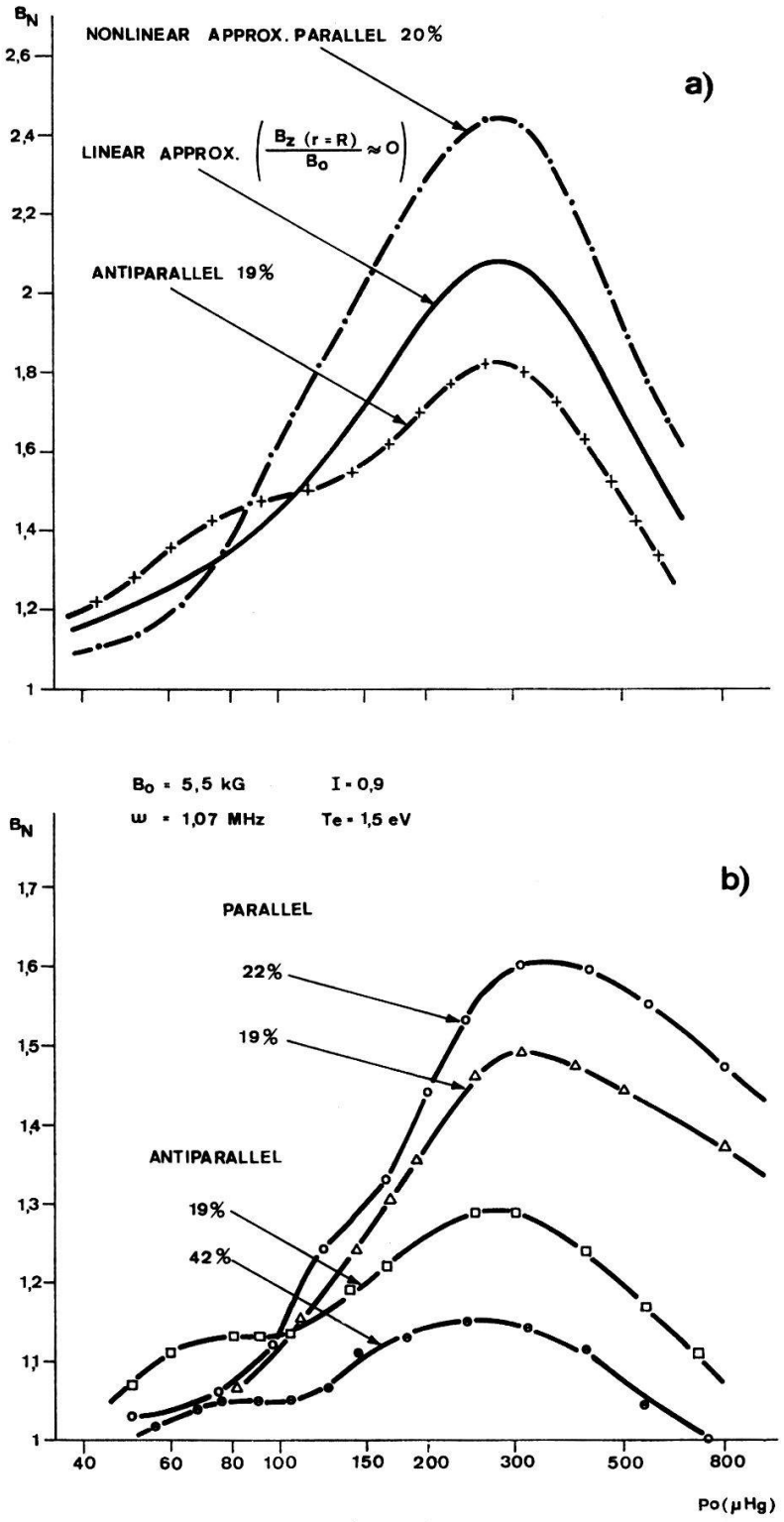

Figure 7

a) Theoretical, b) experimental curves of B_N as a function of p_0.
The parameter of the curves is $B_z(r = R)/B_0$.

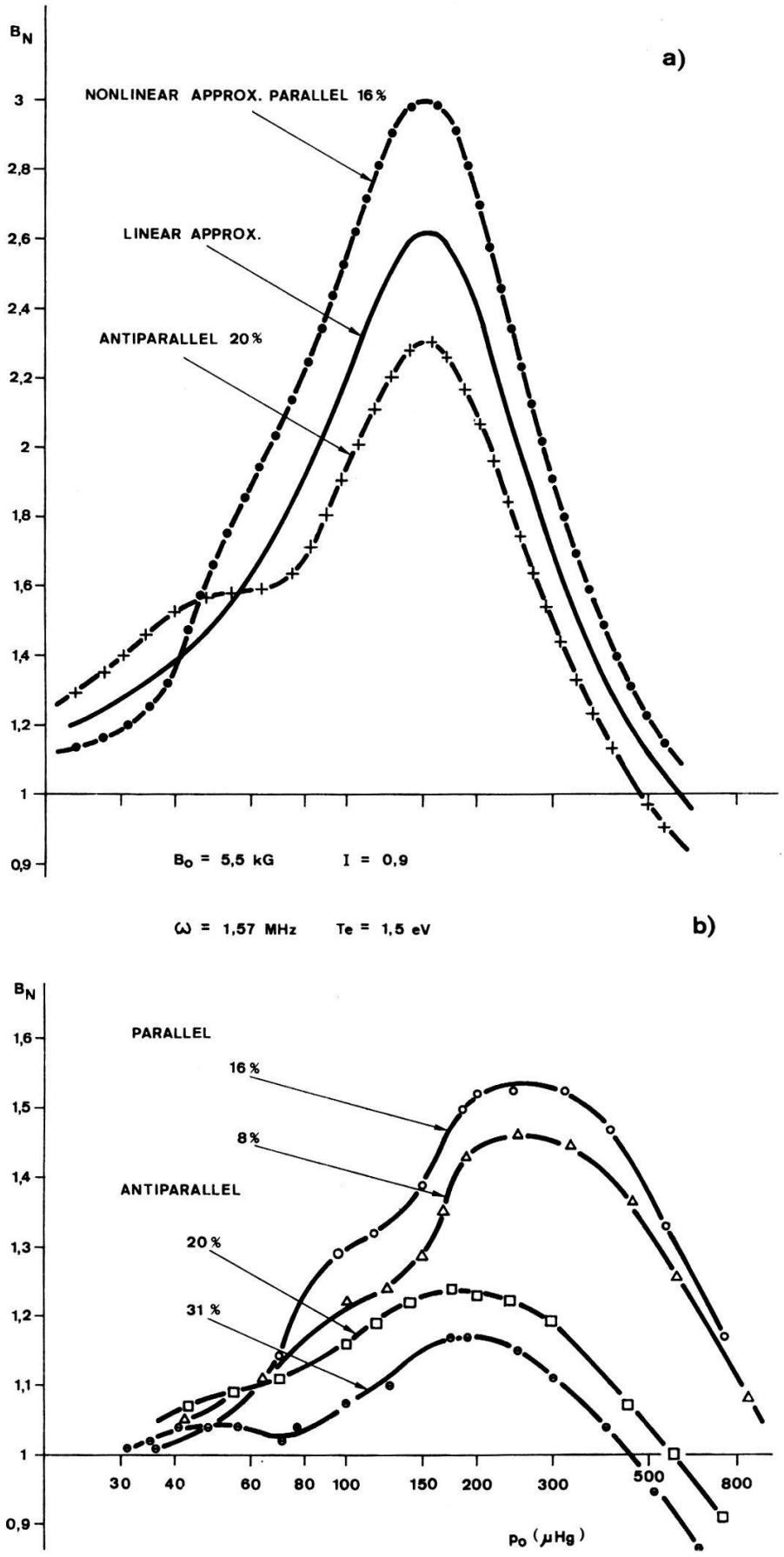

Figure 8

a) Theoretical, b) experimental curves of B_N as a function of p_0. The parameter of the curves is $B_z(r = R)/B_0$.

First, the B_N values were measured as a function of the gas pressure for different combinations of B_0, ω with $B_z\,(r = R)/B_0$ as parameter. Then, the B_N values were measured as a function of $B_z\,(r = R)/B_0$ for the resonance pressure, with degree of ionisation I and B_0, ω combinations as parameters.

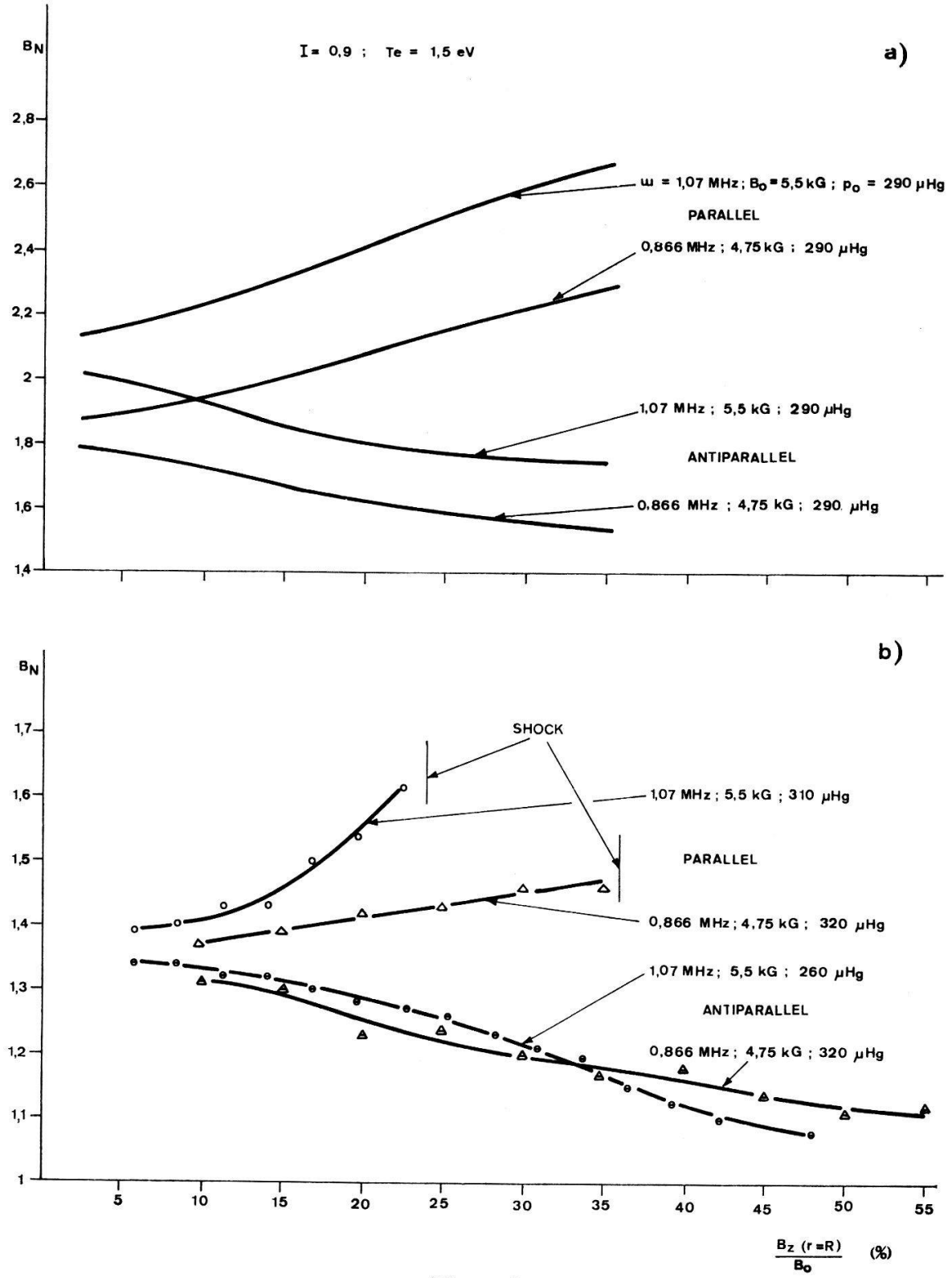

Figure 9

a) Theoretical, b) experimental curves of B_N in the resonance as a function of $B_z(r = R)/B_0$ for different values of B_0 and ω.

Experimental results are shown in Figure 5, 6, 7b, 8b, 9b and 10b. For antiparallel B_0, B_z polarity, the amplitude B_N, as a function of the gas pressure p_0, shows a second peak aside from the main maximum usually observed in linear region. This second peak corresponds to the second harmonics generated by nonlinear effects (Figs. 5, 7b, 8b). The main maximum decreases and vanishes with increasing excitation

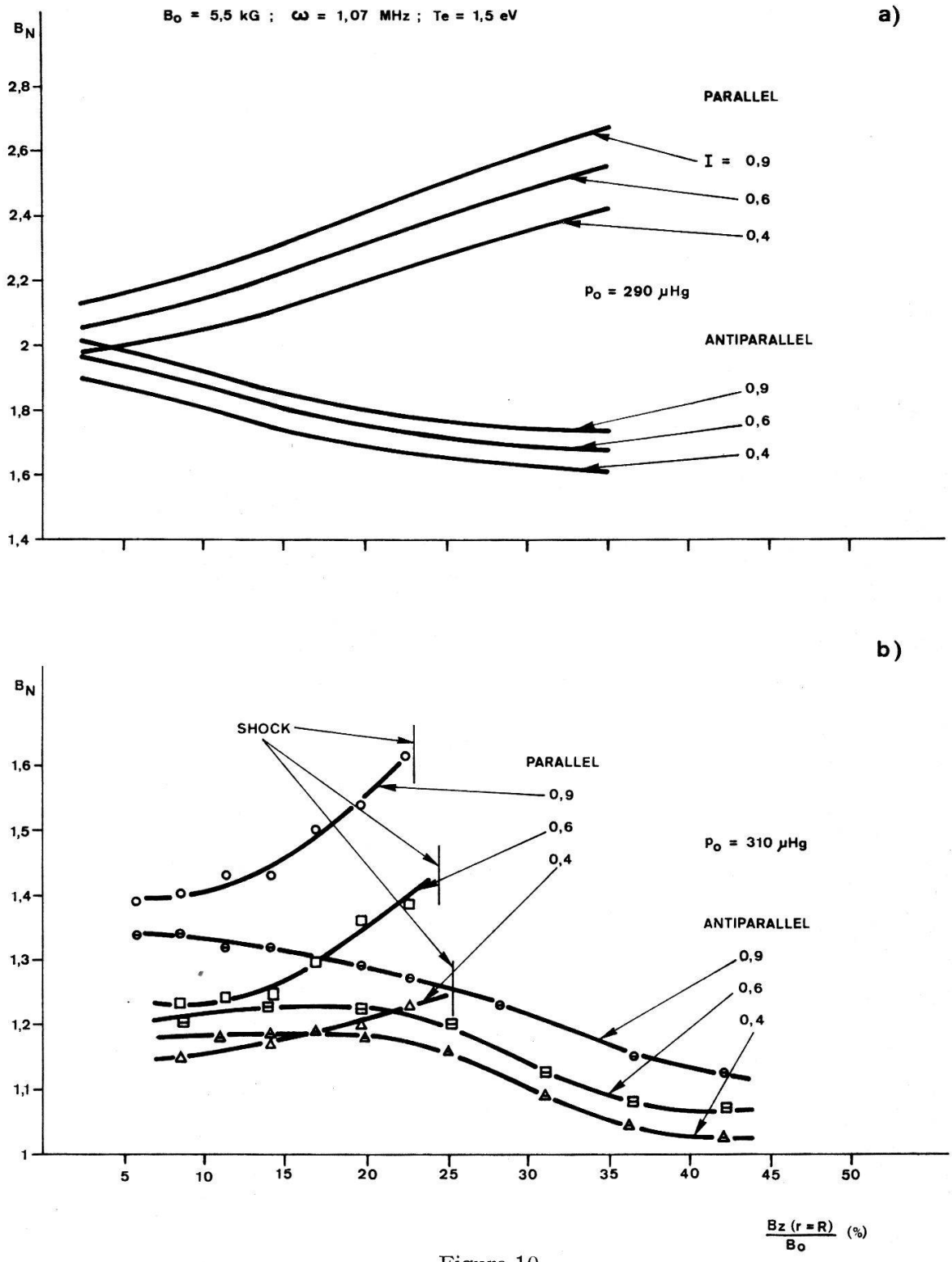

Figure 10

a) Theoretical, b) experimental curves of B_N in the resonance as a function of $B_z(r = R)/B_0$. The parameter of the curves is degree of ionisation I.

energy (Figs. 6, 9b). In the case of parallel B_0, B_z polarity, the nonlinear effects lead only to a deformation of the resonance curve (Figs. 5, 7b, 8b), the main maximum being increased untill shock occurs. The behaviour of the maximal amplitude for both cases in dependance on I, B_0, ω is shown in Figures 9b, 10b.

Comparison of theoretical and experimental curves shows: In the resonance the experimental values of the amplitude are too low as compared with theoretical ones. This discrepancy may be caused by the finite length of the cylinder whereas in theory the infinite length was assumed. For antiparallel polarity, the theoretical and experimental resonance positions are in good agreement (Figs. 7, 8); for parallel

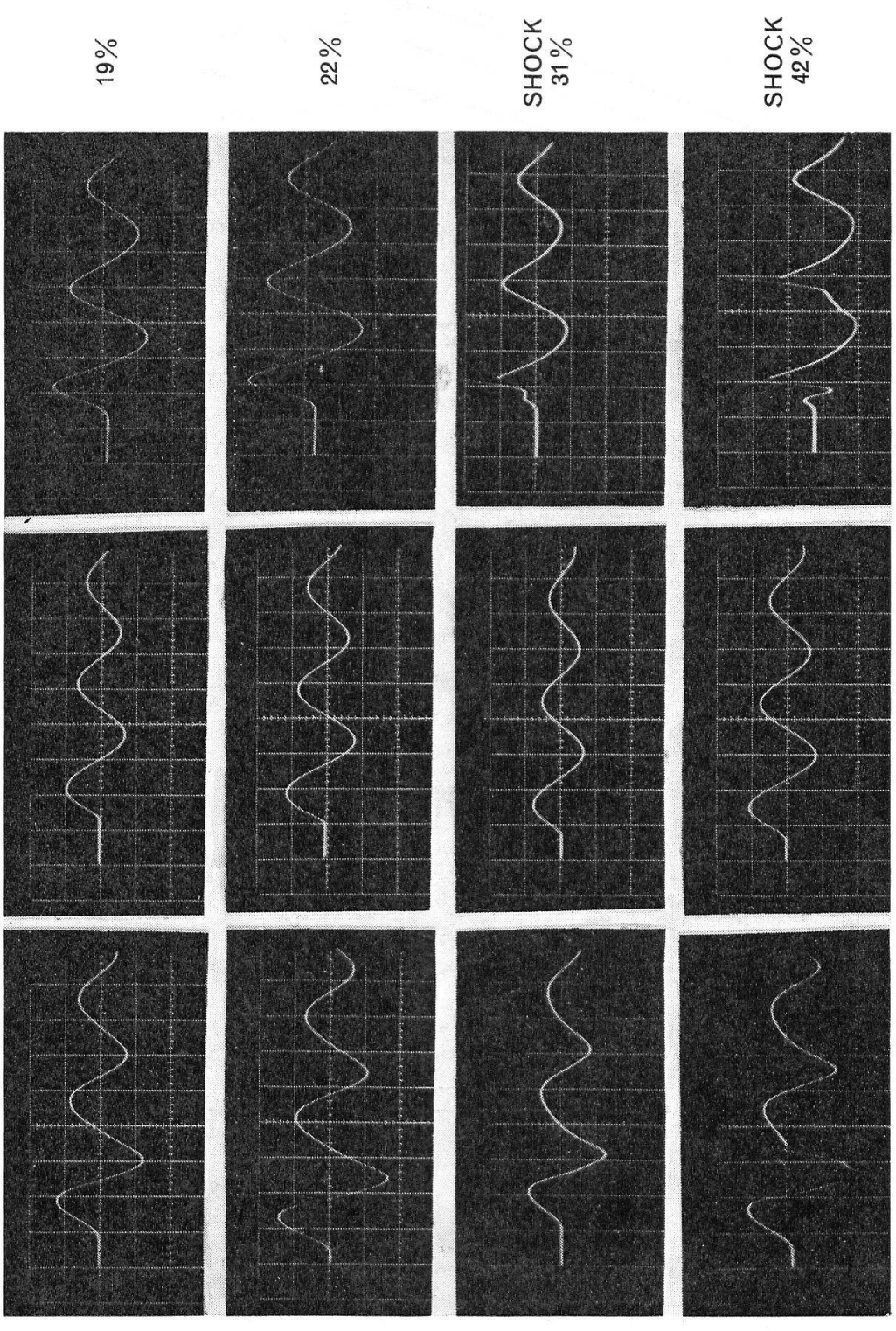

Figure 11
Typical photographs of received signals.

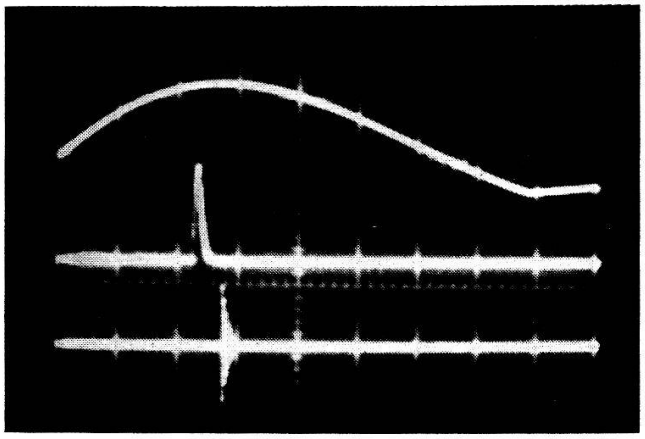

Figure 12

Time sequence of the discharges. The horizontal scale is 200 μsec/div.

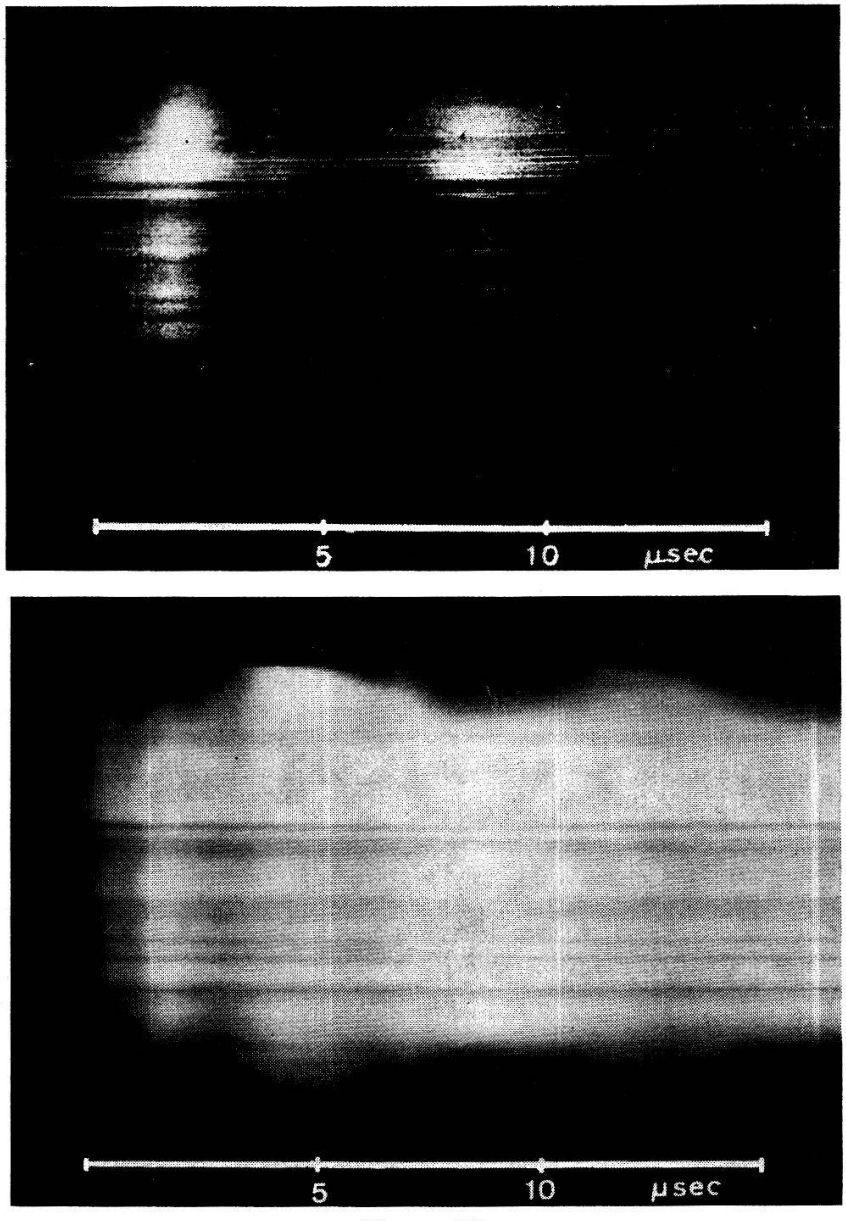

Figure 13

Streak camera photographs of plasma during the excitation for $B_z(r = R)/B_0$ equal to 25% and 50% (shock).

polarity the position of the experimental main maximum is shifted to higher pressures in comparison with the position of the theoretical ones. In our opinion, the cause of this shift is the heating of the plasma by the waves excited. This explanation is based on the following arguments: First, in the theoretical curves computed for higher temperatures (Fig. 2), the position of the main maximum is shifted in the same direction. On the other hand, the more effective heating was observed for higher magnetic field amplitudes in the case of B_0, B_z parallel polarity. The experimental evidence of this heating is given in the forthcoming section.

The above described effects can be seen immediately in the set of oscillogramms shown in Figure 11: the decreasing of B_N for antiparallel, the increasing of B_N and the start of shock for parallel polarity.

3. *Electron Temperature of Disturbed Plasma*

A change of electron temperature caused by excitation was observed by means of streak camera pictures and measured by line intensity measurements.

Time spread photographs made by a streak camera during the excitation show a change of light intensity following the excitation frequency. This effect is more intensive for higher exciting fields. The start of shock wave was also observed (Fig. 13).

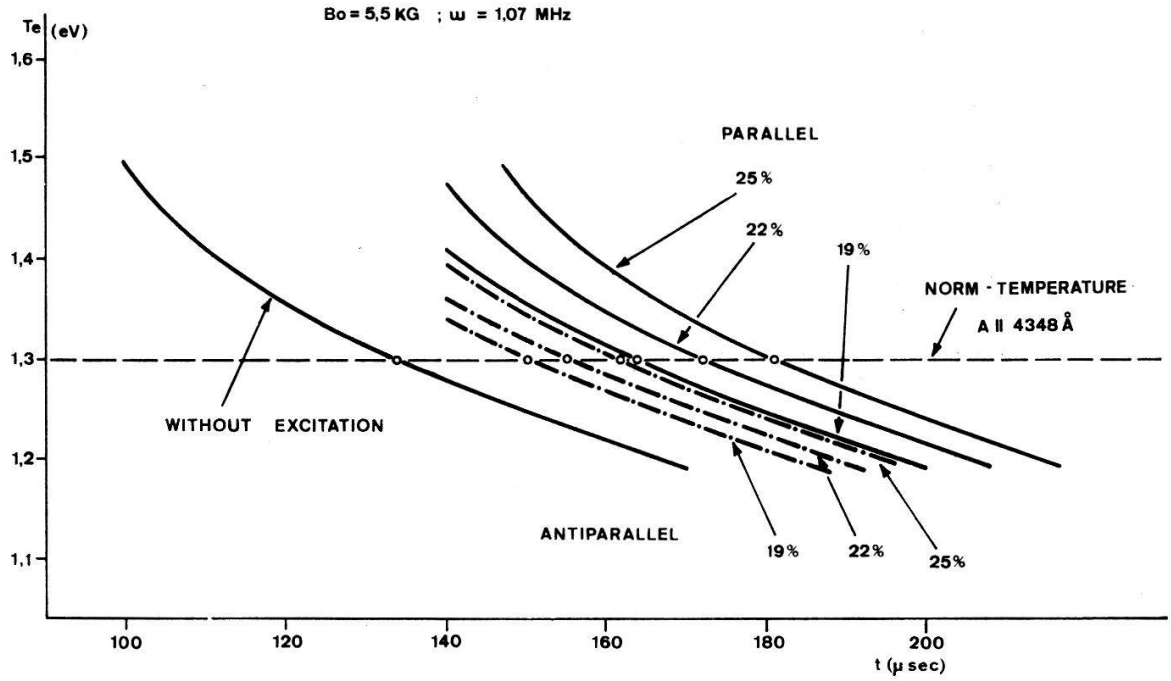

Figure 14

Time dependent temperature curves for different excitation energies and polarities.

The increase of the temperature caused by the waves during the whole time of the excitation was deduced from norm temperature measurement. The A_{II} 4348 line intensity as a function of time was registered for different energies and polarities. The results are shown in Figure 14. The time shift of the intensity maximum is plotted on the norm temperature line. Assuming that after the excitation (140 μsec) the plasma follows the same temperature decrease law as has been described in Section IV.1,

the time dependent temperature curves were extrapolated. From these curves it can be seen that heating is proportional to energy of excitation and higher for parallel polarity.

V. Conclusions

We have studied properties of magnetoacoustic resonance, both theoretically and experimentally, in the region where the exciting field amplitude is not small compared with the magnetostatic field. The dependence on the mutual polarity of B_0, B_z and on the exciting energy was found and excitation of higher harmonics was observed. The general agreement between theoretical and experimental results indicates that the theory adequately describes the phenomena. The small discrepancies may be due to the finite length of the cylinder whereas in the theory the infinite length was assumed. Furthermore, in the theory only second order electrodynamical nonlinearities and changes of plasma parameters assumed as constant undoubtedly occur. Nevertheless, we think that our results contribute to the general understanding of nonlinear wave processes in plasma.

Acknowledgments

We want to thank Prof. O. HUBER for his continued interest, discussion and support in this work. Furthermore we would like to thank Mr. B. HOEGGER for the construction of the excitation circuit, and Mr. P. WINIGER and Mr. H. SCHNEUWLY for advice in programming.

References

[1] D. A. FRANK-KAMENETSKII, Soviet Phys.-JETP *12*, 469 (1961).
[2] D. A. FRANK-KAMENETSKII, Soviet Phys.-Techn. Phys. *5*, 847 (1961).
[3] I. A. KOVAN et al., Zh. Eksp. i Teor. Fiz. *43*, 16 (1962).
[4] A. V. BORODIN et al., Nucl. Fus. *3*, 38 (1963).
[5] E. CANTIENI, H. SCHNEIDER, Helv. phys. Acta *36*, 993 (1963).
[6] S. I. BRAGINSKII, Rev. Plasma Phys., Edit. by M. A. Leontovich, Consultants Bureau, New York, *1* (1965).
[7] M. MORSE, H. FESHBACH, *Methods of Theoretical Physics* (McGraw-Hill Book Company Inc., 1953).
[8] B. HOEGGER, Diplomarbeit, University of Fribourg, (1967) unpublished.
[9] R. ROMPE, M. STEENBECK, *Ergebnisse der Plasmaphysik und der Gaselektronik* (Akademie-Verlag, Berlin), *1* (1967).
[10] D. E. T. F. ASHBY, D. F. JEPHCOTT, Appl. Phys. Lett. *3*, 13 (1963).